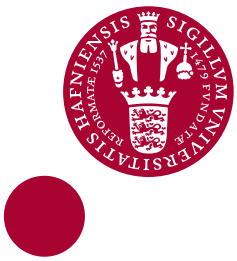

Convective Self-Aggregation As a Cold Pool-Driven Critical Phenomenon

Haerter, Jan O.

Published in:
Geophysical Research Letters

DOI:
10.1029/2018GL081817

Publication date:
2019

Document version
Publisher's PDF, also known as Version of record

Geophysical Research Letters

RESEARCH LETTER
10.1029/2018GL081817

Convective Self-Aggregation As a Cold Pool-Driven Critical Phenomenon

Jan O. Haerter[1]

[1]Niels Bohr Institute, University of Copenhagen, Copenhagen, Denmark

Key Points:
- Convective self-aggregation can result from cold pool interaction and global energy constraints alone
- A model is presented, which shows a phase transition between a uniform state and an aggregated state, as cold pool interaction is increased
- The phase diagram is mapped out in 2-D space spanned by spontaneous generation and interaction strength, showing where aggregation dominates

Supporting Information:
- Supporting Information S1

Correspondence to:
J. O. Haerter,
haerter@nbi.ku.dk

Citation:
Haerter, J. O. (2019). Convective self-aggregation as a cold pool-driven critical phenomenon. *Geophysical Research Letters*, *46*, 4017–4028. https://doi.org/10.1029/2018GL081817

Received 22 DEC 2018
Accepted 27 MAR 2019
Accepted article online 1 APR 2019
Published online 8 APR 2019

Abstract Convective self-aggregation is when thunderstorm clouds cluster over a constant temperature surface in radiative convective equilibrium. Self-aggregation was implicated in the Madden-Julian Oscillation and hurricanes. Yet, numerical simulations succeed or fail at producing self-aggregation, depending on modeling choices. Common explanations for self-aggregation invoke radiative effects, acting to concentrate moisture in a subdomain. Interaction between cold pools, caused by rain evaporation, drives reorganization of boundary layer moisture and triggers new updrafts. We propose a simple model for aggregation by cold pool interaction, assuming a local number density $\rho(\mathbf{r})$ of precipitation cells, and that interaction scales quadratically with $\rho(\mathbf{r})$. Our model mimics global energy constraints by limiting further cell production when many cells are present. The phase diagram shows a continuous phase transition between a continuum and an aggregated state. Strong cold pool-cold pool interaction gives a uniform convective phase, while weak interaction yields few and independent cells. Segregation results for intermediate interaction strength.

1. Introduction

Drawing a link between cloud and precipitation processes and statistical mechanics is intriguing: Similar to the characteristics of critical phenomena (Yeomans, 1992), cloud fields often show long-ranged correlations and near-fractal scaling (Cahalan & Joseph, 1989; Lovejoy & Schertzer, 2006). The possibility that the cloud field might have scaling properties is appealing because this might imply universal behavior, where only few features of the small-scale interactions are relevant in capturing emergent organization (Goldenfeld, 2018). Invoking nonequilibrium statistical physics, a relation to the sand pile model (Bak et al., 1987) has been drawn, which coins the notion of *self-organized criticality*. Loosely speaking, precipitation could be ascribed characteristics of an avalanche, when moisture, brought into a domain of interest, is abruptly released after a critical mixing ratio is exceeded (Peters & Christensen, 2002; Peters & Neelin, 2006).

A particularly appealing candidate for critical behavior is the radiative convective equilibrium framework (Held et al., 1993). Radiative convective equilibrium requires overall constant and homogeneous boundary conditions, for example, constant surface temperature and moisture as well as insolation, and that the energy fluxes entering and leaving the system be equal. Under such conditions, humidity perturbations have repeatedly been shown to grow over time, in a process termed convective self-aggregation (Bretherton & Khairoutdinov, 2015; Bretherton et al., 2005; Coppin & Bony, 2015; Holloway et al., 2017; Jeevanjee & Romps, 2013; Muller & Held, 2012; Muller & Bony, 2015; Wing et al., 2017). Explanations have in common that a feedback must exist, by which already moist regions grow moister, while dry regions become even drier. One possible mechanism is that cloudy regions lose less heat through long-wave radiation than do cloud-free regions. In this process, subsidence would buildup over the cloud-free regions, leading to low-level divergence there and suppression of cloud and precipitation. In some observational work, however (Tobin et al., 2012), no strong sensitivity of the radiative budget at the top of the atmosphere to self-aggregation has been found.

Here, we use equilibrium statistical physics only as an analogy, but follow a dynamical systems approach. Taking large-scale organization as an emergent aspect from the small scales, we test whether interactions between convective updrafts can give rise to system-scale organization. Cold pools, resulting from evaporative cooling under precipitating convective clouds, spread as gravity currents away from the center of the precipitation cell. At the scale of ~10 km, cold pool gust fronts have been shown to stimulate the initiation of new convective updrafts (Böing, 2016; de Szoeke et al., 2017; Feng et al., 2015; Grant & van den Heever,

2016; Grabowski, 2001; Haerter & Schlemmer, 2018; Langhans & Romps, 2015; Romps & Jeevanjee, 2016; Tompkins, 2001a, 2001b; Terai & Wood, 2013; Torri & Kuang, 2018; Zuidema et al., 2017). Cold pools can reach maximal radii of r_{max} ~10–100 km over sea surfaces, and travel at an initial radial velocity of ~5 m/s, which is however gradually reduced in the course of their lifetimes (Black, 1978; Feng et al., 2015; Romps & Jeevanjee, 2016; Zuidema & Li, 2012). It is increasingly appreciated that correlations exist between the locations of present precipitation cells and those of subsequent ones, likely mediated through cold pool activity (Böing, 2016; de Szoeke et al., 2017; Haerter et al., 2018; Torri & Kuang, 2018; Windmiller, 2017) and that precipitation can widen the distribution function of boundary layer buoyancy (Haerter & Schlemmer, 2018). In recent work (Haerter et al., 2018; Torri & Kuang, 2018), it was shown that the collision between cold pools is the dominant process of generating new convective events—activation by isolated gust fronts without collision may be of second order. Interestingly, strong cold pool activity was stated to hamper the buildup of a self-aggregated state in simulations (Jeevanjee & Romps, 2013), while cold pools are indeed ubiquitous in regions of precipitating convection (Zuidema et al., 2017), in particular in cases of deep convection.

We therefore ask, how much a convective cloud system can self-organize into an aggregated state, if cold pool interactions are the relevant process leading to new convective cells? In recent conceptual and simulation work (Haerter et al., 2018), the detailed interactions between cold pools were considered. It was shown, by the analysis of large-eddy simulations, that it is most often collisions between several colliding cold pool gust fronts, rather than individual gust fronts, that set off new convective updrafts. In describing the positions of new cells by a simplified geometrical model, positions were taken to be precisely defined, for example, when growing cold pool gust fronts collided, the new cell was produced at the first point of intersection between the gust fronts.

Here, we first relax the requirement that new cells must occur at precisely defined points. In other words, we take new cells to emerge *near* gust front collisions of existing cold pools, but allow the new cells to be displaced by a random distance of the order of the typical cold pool radius. Such displacement has indeed been mentioned in early work (Tompkins, 2001a), where new cells emerge somewhat randomly, but generally along the line of collision between two previous cold pool gust fronts.

Such spatial randomness allows us to start from the assumption that cold pool interactions can be modeled by only the number density, rather than explicit positions, of cell centers in a given local environment. The continuum model we derive enables us to map out a phase diagram of aggregation. In a second step, we again tighten the assumptions, and return to microscopic correlations, where new cells do have a precisely defined position relative to the ones causing them. We contrast this refined model to the continuum model. Our results support the key conclusion that, in both types of models, collisions between cold pools can lead to convective self-aggregation while single cold pool triggering alone cannot. Radiative effects are only required in a domain-average sense, in order to constrain the total system energy flux.

2. Results

2.1. Model

As our conceptual model aims to incorporate a global energy constraint, the heat entering the atmosphere through the lower boundary (e.g., a tropical sea surface) should leave at the top. Our model considers this energy flux by assuming that heat is transported to the cloud layer through latent heating during cloud formation (Figure 1a). It further assumes that heat within the cloud layer will equilibrate relatively fast with the surroundings through comparably rapid gravity waves (Bretherton & Smolarkiewicz, 1989). All heat transported to the cloud layer is eventually radiated out to space by long-wave radiative emission. We simply mimic the global energy constraint by assigning an equal energy flux ϵ to each convective cloud and refer to the total system energy flux as $\mathcal{E}$.

The model domain is a square of linear dimensions $L_x = L_y = L$ and an effective elementary area a is required for each precipitation cell. a necessarily includes the precipitation cell itself, but also further effects that inhibit other precipitation cells from populating this area at the same time. This could be downbursts or strong temperature depressions caused near the precipitation cell. We additionally define an (generally larger) area unit, $a_{cp} = \pi r_{max}^2$, as the area that a cold pool gust front can cover, if its maximum radius is r_{max}. As mentioned, r_{max} ~10–100 km, which is larger than the updraft shaft and downburst area, but substantially smaller than the domain area, that is,

$$a < a_{cp} \ll L^2 \,. \tag{1}$$

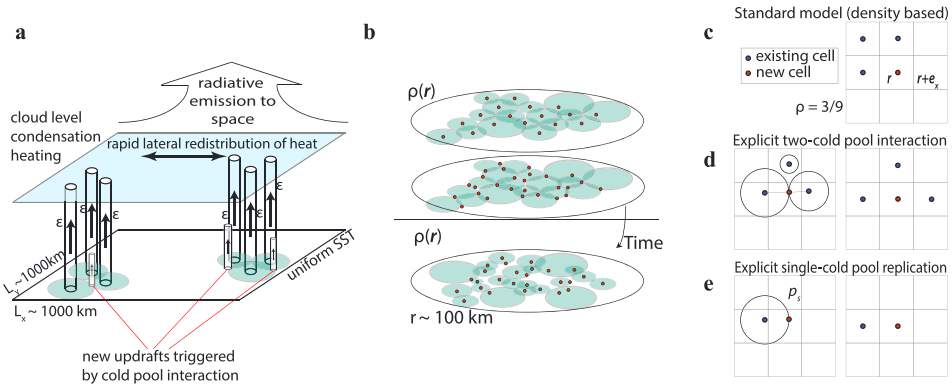

Figure 1. Simple model for organization through cold pools. (a) Schematic of cloud system, with vertical columns showing updrafts of energy flux ϵ each, cold pools (green ellipses at the surface), new cells created by cold pools (small columns), as well as the cloud level. SST = sea surface temperature. (b) Details of local cold pool interaction (lateral scale ~100 km): Schematic shows precipitation cell centers (red points) and their corresponding cold pools (green), where at a given time step cold pools spread and form new cells near points of interference. $\rho(\mathbf{r})$ is the number density of cells within the subdomain shown. The process continues at the subsequent time step, with cold pools again emanating from the new cell centers. (c–e) Distinguishing processes: (c) Purely density-based formulation: The probability of the central lattice site becoming occupied is proportional to the density $\rho(\mathbf{r})$ of occupied sites in its surroundings. In the example shown, r_{max} is chosen so that all eight neighboring sites contribute to the density, that is, $\rho(\mathbf{r}) = 1/3$, since three neighboring sites are occupied (blue). (d) Explicit two cold pool interaction: A new cell can be set off only if the lattice site $\mathbf{r}$ lies between any of the neighboring lattice sites. In the example shown, a new cell is possible, since blue cells lie both to the left and right of the site $\mathbf{r}$. The circles indicate possible cold pool gust fronts. (e) Explicit single cold pool replication: A new cell is possible within the neighborhood of an existing cell.

The domain total number of precipitation cells is expressed as N. Specifically, listing all horizontal positions (2-D) of precipitation cells as $\mathbf{c}_i$ we can write

$$N \equiv \int_{\mathbf{r}} d\mathbf{r} \sum_i \delta(\mathbf{r} - \mathbf{c}_i) \,, \tag{2}$$

where δ is the Dirac delta function and the integral is taken over the entire domain.

The domain mean number density $\overline{\rho} \equiv N/N_{max}$ with $N_{max} \equiv L^2/a$ the maximal number of cells. $\overline{\rho}$ is hence the probability of finding a given elementary area a occupied by a precipitation cell. The total energy flux then is $\mathcal{E} = N\epsilon$, but we will generally simply work in units of total number density $\overline{\rho}$, as all our rain cells have equal energy flux. Analogously to equation (2), at any given position $\mathbf{r}$, we also define a local number density

$$\rho(\mathbf{r}) \equiv a\, a_{cp}^{-1} \int_{r=0}^{r_{max}} \int_{\phi=0}^{2\pi} dr d\phi \sum_i \delta(\mathbf{r} + \mathbf{r}' - \mathbf{c}_i) \,, \tag{3}$$

with $\mathbf{r}'(r, \varphi) \equiv (r\,cos(\varphi), r\,sin(\varphi))$ Equation (3) specifies the number density of cold pools which may affect the point $\mathbf{r}$ (Figures 1b and 1c), since the integral in equation (3) regarding r is taken within the range $0 < r < r_{max}$, that is, the maximal radius within which one cold pool can collide with another. Only to avoid possible confusion, we emphasize that the symbols ρ and $\overline{\rho}$ are here used as number densities, whereas, in other contexts, the symbol ρ sometimes denotes the density of air within and surrounding cold pools.

To describe the dynamics of $\rho(\mathbf{r})$ we consider three dynamical processes: (i) spontaneous cell production; (ii) cell decay; and (iii) cell interactions.

- *Spontaneous cell production* occurs for sufficient atmospheric instability and space for cells to emerge. To incorporate the former, the rate of spontaneous production is tied to the total energy flux by making the spontaneous production $\sim f_{sg}\,(1 - \overline{\rho})$. Lower rates of spontaneous production hence occur when the domain mean flux is already large. $f_{sg} \geq 0$ is thereby a parameter controlling the disorder, or random seeding of cells, in the system. As downdrafts and cooling through rain evaporation effectively reduce the buoyancy near a given cell center after a precipitation event has occurred (Feng et al., 2015; Moseley et al., 2018), a limitation on the space available to new cells should be incorporated in the model. This

is accomplished by the additional factor $1 - \rho(\mathbf{r})$, which ensures that each vacant area a has the same probability of experiencing a spontaneous event. In total, spontaneous growth evolves as $f_{sg}(1-\overline{\rho})(1-\rho(\mathbf{r}))$.

- *Cell decay* occurs for each cell present at an equal rate $f_d \equiv \tau_d^{-1}$, where $\tau_d > 0$ is the effective duration of a precipitation event (in practice, Feng et al., 2015; Moseley et al., 2018, τ_d is on the order of 1 hr). Local cell density $\rho(\mathbf{r})$ hence evolves as $-f_d\rho(\mathbf{r})$, leading to exponentially decaying cell populations if all other processes were absent.
- *Cell interaction* is due to cold pool processes. For all vacant areas in the vicinity of $\mathbf{r}$, that is, $\sim (1 - \rho(\mathbf{r}))$, the cold pools emanating from all cells present within a radius r_{max} around $\mathbf{r}$ can help instigate a new cell at $\mathbf{r}$. We therefore introduce an effective probability $p_0 \geq 0$ for cold pools in the vicinity to collide at position $\mathbf{r}$. The cell production from cold pool interaction is then modeled by $P_0(\overline{\rho})\rho(\mathbf{r})^m(1-\rho(\mathbf{r}))$, where the probability $P_0(\overline{\rho}) = p_0(1 - \overline{\rho})$ again warrants the total energy constraint. Large values of p_0 mean that cold pools are more efficient at generating new cells. It is important to understand the meaning of the exponent m, which serves to distinguish cold pool processes resulting from one or multiple cold pools: $m = 1$ describes a process where replication is proportional to the density $\rho(\mathbf{r})$, that is, each cold pool replicates at a rate that is independent of the presence of others. $m = 2$ describes processes that involve collisions, that is, the replication of one cold pool depends on the presence of others in the surroundings. The general ability of cold pool collisions to trigger new convective cells (Droegemeier & Wilhelmson, 1985; Feng et al., 2015; Tompkins, 2001a; Torri & Kuang, 2019), and the explicit comparison between $m = 1$ and $m = 2$, suggest a crucial role of collision effects between distinct cold pool gust fronts (Haerter et al., 2018).

Note that our key assumption, which will be relaxed in section 2.2.4, is that cold pool interaction is a purely density dependent process. Geometrical constraints and morphologies of cell organization are hence considered higher-order corrections. Such an assumption of a *density field* would be justified, when collisions between cold pools are sufficiently noisy, meaning that new cells are never produced precisely at the position of collision. Hence, in our model the number of cold pools contributing to the production of a new cell is relevant, but not the detailed position of the cell produced—justifying a coarse-grained density field $\rho(\mathbf{r})$ near the point of collision.

Piecing together the three processes above, the complete dynamical equation describing the evolution of cell density $\rho(\mathbf{r}, t)$ is

$$\frac{d}{dt}\,\rho(\mathbf{r},t) = p_0(1-\overline{\rho})\rho(\mathbf{r})^m(1-\rho(\mathbf{r})) + f_{sg}(1-\overline{\rho})(1-\rho(\mathbf{r})) - f_d\,\rho(\mathbf{r}) \tag{4}$$

$$= (1-\overline{\rho})(1-\rho(\mathbf{r}))(p_0\,\rho(\mathbf{r})^m + f_{sg}) - f_d\,\rho(\mathbf{r})\,. \tag{5}$$

For subsequent use, we express all rates in units of f_d. This is accomplished by dividing equation (5) through by the precipitation frequency f_d (inverse duration of a precipitation event). This amounts to the replacements $p_0 \to p_0/f_d, f_{sg} \to f_{sg}/f_d, f_d \to 1$, leaving p_0 and f_{sg} as the remaining parameters. Time is now measured in units of precipitation duration, and space in units of a (defined above). Furthermore, we define $q \equiv 1-\overline{\rho}$ and, from now on, drop the explicit reference to the argument $\mathbf{r}$ of ρ, taking the symbol ρ to always refer to local cell density, as opposed to $\overline{\rho}$, which measures the system average density. We can then more compactly define the RHS of equation (5) as

$$F_{q,p_0,f_{sg}}(\rho) \quad \equiv \quad q\,(1-\rho)(p_0\,\rho^m + f_{sg}) - \rho\,. \tag{6}$$

To make the analogy to a critical phenomenon more explicit, we note that, as a polynomial in ρ, equation (6) can be interpreted as the derivative of a potential, denoted $V_{q,p_0,f_{sg}}(\rho)$, where $F_{q,p_0,f_{sg}}(\rho) = -d\,V_{q,p_0,f_{sg}}(\rho)/d\,\rho$. For $m = 2$, $V_{q,p_0,f_{sg}}(\rho)$ becomes of fourth order in ρ and can exhibit two competing local minima.

A few comments are appropriate:

(i) The growth limitation by the factor $q = 1-\overline{\rho}$ is analogous to that for logistic growth in population dynamics, where the term is interpreted as a total resource limitation; the term $(1 - \rho)$ has a similar effect, but encodes local space limitations. The factor $(1 - \rho)$ takes into account that two cold pools cannot be in the same location, which is reminiscent of the repelling force in a Van der Waals Gas of particles with a finite radius. Conversely, for $m = 2$ the generation of new cold pools by ρ^m in equation (6) is promoted

by having two cold pools in each other's vicinity, giving a competing effect between space limitation and growth.

(ii) The factor $p_0\rho^m + f_{sg}$ is crucial in describing the local dynamics of cell growth. For sufficiently low density ρ, spontaneous cell production is dominant, while for large ρ, most new cells are produced by cold pool interactions.

(iii) For bistable steady state solutions to equation (5), the exponent m should be larger than unity. To see this, consider that for $m = 1$, $F_{q,p_0,f_{sg}}(\rho) = q(1-\rho)(p_0\rho + f_{sg}) - \rho$ is quadratic in ρ and therefore can only have a single stable fixed point. More explicitly, $F_{q,p_0,f_{sg}}(1) = -1$ and $F_{q,p_0,f_{sg}}(0) = q f_{sg} \geq 0$. Hence, depending on the choices of p_0 and f_{sg}, there is (a) either a unique stable fixed point at $\rho \leq 0$ (negative ρ is even unphysical) or (b) a unique stable fixed point at a density $0 < \rho < 1$. For $m = 2$, which we will discuss in detail in the following, the steady state expression of equation (5) is of third order in ρ and bistability becomes possible for certain parameter combinations.

2.2. Self-Aggregation

2.2.1. Definition

In some studies, an increase in the spatial variance of cloud or liquid water has been employed as a measure of self-aggregation. However, this measure would still allow for many disconnected cloud clusters. Here, we want to define self-aggregation as the state where, in the limit of $t \to \infty$, complete segregation of the domain into a cloudy and a noncloudy component takes places. To quantify this, we will subsequently use the number densities of convective cells within the different phases.

2.2.2. Case Without Spontaneous Generation

Consider the case of $f_{sg} = 0$, a situation where new cells are exclusively produced by cold pool collisions. We are interested in the range of parameters, where a fully aggregated state can be stable. To make progress, we check for the stability of two bulk phases and the boundary between these bulk phases: The two bulk phases consist of the stable solutions to equation (5), where the density is either high or low. Using that $f_{sg} = 0$, equation (5) simplifies to

$$\dot{\rho} = F_{q,p_0}(\rho)\,, \tag{7}$$

$$F_{q,p_0}(\rho) \equiv -\rho\, q\, p_0\, (\rho^2 - \rho + 1/(q\, p_0))\,. \tag{8}$$

Looking for local solutions in dependence on q, apart from the trivial solution $\rho_1 = 0$, we obtain

$$\rho_{2,3} = \frac{1}{2} \mp \left(\frac{1}{4} - \frac{1}{p_0 q}\right)^{\frac{1}{2}}\,. \tag{9}$$

Equation (9) offers physically meaningful solutions for $p_0 q \geq 4$. Both ρ_1 and ρ_3 are stable fixed points, which we check by verifying that $\partial F_{q,p_0}/\partial\rho|_{\rho=\rho_{1,3}} < 0$.

So far, we have treated $q \equiv 1 - \overline{\rho}$ as a parameter. However, q should be obtained in such a way that the partitioning of the domain into regions of high and low density (ρ_3 and ρ_1, respectively) is stable. One therefore has to consider the interface between these two regions of densities ρ_1 and ρ_3, respectively, and demand that the density at the interface be constant (Figure 2a). As an approximation, consider the interface to locally be a straight line boundary, that is, we neglect its curvature and consider that the interface is smooth and sharp, so that for one half plane $\rho = \rho_1 = 0$, for the other, $\rho = \rho_3$, as given by equation (9). This straight line approximation is valid, as long as r_{max} is far smaller than the radius of the aggregated subdomain. For finite-size systems the curvature can generally not be neglected and should be treated as a correction. We describe the effective density for any point at the interface as the average $\rho_{ave} \equiv (\rho_1 + \rho_3)/2 = \rho_3/2$, and further that ρ_{ave} be constant, that is,

$$F_{q,p_0}(\rho_{ave}) = 0\,, \tag{10}$$

or, equivalently,

$$\rho_2 = \rho_3/2\,. \tag{11}$$

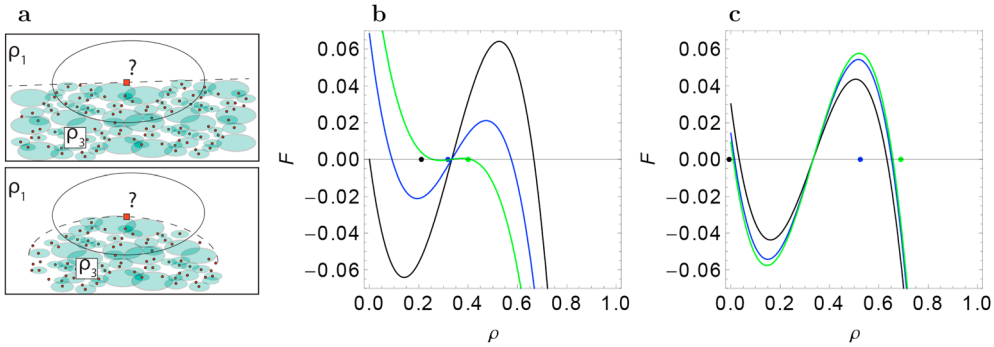

Figure 2. Fixed points for different models. (a) Schematic exemplifying the effect of an infinite boundary (approximately straight line boundary), versus a finite boundary, which then shows a pronounced curvature affecting the replication probability at the boundary. The red square indicates a point at the boundary, which uses the density computed within the circled area, to determine a possible update. (b) Model with quadratic dependence on ρ, that is, $m = 2$ in equation (5), where $q = 9/2(9f_{sg} + p_0)$ is chosen to ensure that $\rho_1 + \rho_3 = 2\rho_2$, that is, that an aggregated state is possible. Black, blue, and green curves correspond to increasing values of $f_{sg} = \{0, 0.1, 0.2\}$, respectively, with fixed $p_0 = 5.7$. Filled circles in corresponding colors along the horizontal axis indicate the corresponding values of $\overline{\rho} = 1 - q$. Note that the value of $\overline{\rho}$ increases with f_{sg} and eventually departs from the allowed range $\rho_1 < \overline{\rho} < \rho_3$. (c) Similar to (b) but for $f_{sg} = .03$ held fixed and $p_0 = \{4.2, 9.2, 14.2\}$ for colors black, blue, and green, respectively. Note that in this example only the intermediate value of p_0 yields a self-aggregated state.

Using this together with equation (9) yields

$$q = 1 - \overline{\rho} = \frac{9}{2} p_0^{-1} , \tag{12}$$

and $\rho_1 = 0, \rho_2 = 1/3, \rho_3 = 2/3$. Hence, if the aggregated state exists, the total cloud-free area q is inversely proportional to the interaction factor p_0 and the density within the cloudy bulk area is independent of q and equal to $2/3$. But for which p_0 can aggregation be expected? Clearly, $\overline{\rho} = 1 - q$, the average density, must lie between the densities of the two phases, hence,

$$\rho_1 < 1 - q < \rho_3 , \tag{13}$$

yielding

$$\frac{9}{2} \equiv p_{0,min} < p_0 < p_{0,max} \equiv \frac{27}{2} . \tag{14}$$

Hence, the segregated phase is limited to intermediate values of p_0. For $p_0 \leq p_{0,min}$, the domain is entirely cloud-free, that is, $\overline{\rho} = 1 - q = 0$. For $p_0 \geq p_{0,max}$, no long-lived cloud-free region will exist. However, transient density fluctuations are possible. Our solution predicts that, for $p_0 \geq p_{0,max}$, $\overline{\rho}$ will follow the uniform bulk solution (inserting $\rho = \overline{\rho} = 1 - q$ and $f_{sg} = 0$ in equation (6)) to

$$F(\overline{\rho}) = p_0(1 - \overline{\rho})^2 \overline{\rho}^2 - \overline{\rho} = 0 , \tag{15}$$

and it is easy to check that for $p_0 \geq p_{0,max}$ there is only one stable, plausible, solution for $\overline{\rho}$. Equation (15) gives $\overline{\rho}(p_{0,max}) = 2/3$, which matches that obtained from equation (12) for the segregated solution, hence $\overline{\rho}(p_0)$ is continuous at $p_{0,max}$. We further check the slopes

$$s_< \equiv \lim_{\substack{p_0 \to p_{0,\max} \\ p0 < p0,max}} \frac{\partial \overline{\rho}}{\partial p_0} = \frac{2}{81} \tag{16}$$

$$s_> \equiv \lim_{\substack{p_0 \to p_{0,max} \\ p_0 > P0,max}} \frac{\partial \overline{\rho}}{\partial p_0} = \frac{4}{243} \tag{17}$$

hence, $s_< > s_>$, signaling a continuous phase transition of $\overline{\rho}(p_0)$ at $p_{0,max}$. We check this result by explicit simulations (Figure 3).

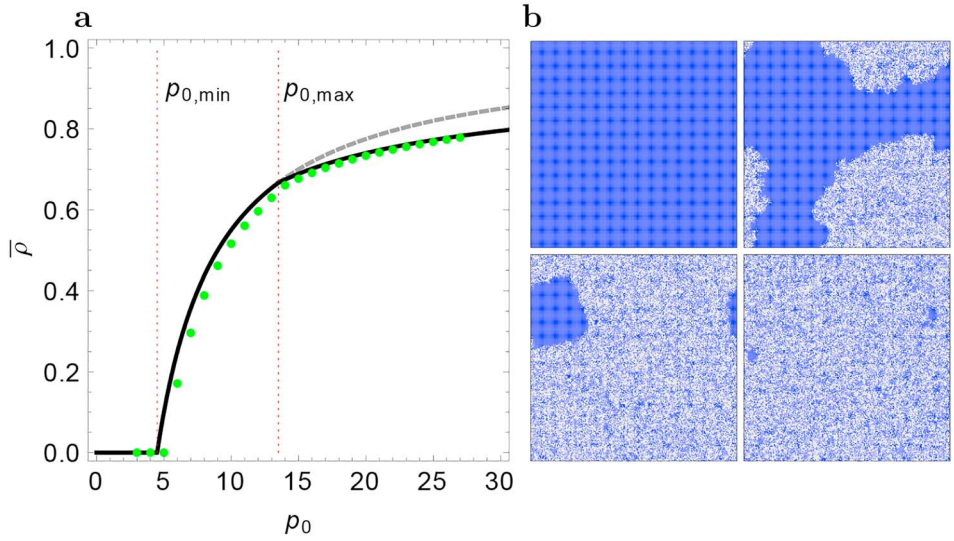

Figure 3. Cloud fraction versus interaction. (a) Cloud fraction $\overline{\rho}$ as a function of p_0 in the case without spontaneous generation ($f_{sg} = 0$). Theoretical and simulation result shown as black line and green points, respectively. Red vertical dotted lines indicate $p_{0,min}$ and $p_{0,max}$, respectively, that is, the limits between which segregation can take place. Gray dashed line is the function $\overline{\rho} = 1 - 9/2p_0$ (valid in the segregated regime), to demonstrate the change of slope at $p_{0,max}$. The slight discrepancy between the theoretical and simulation results is likely due to the assumption of smooth and straight interfaces between the cloudy and cloud-free areas, as well as noise caused by finite size effects and lattice discretization. Simulations were carried out on a lattice of 300 × 300 sites with periodic boundary conditions using a Gillespie algorithm for all rates involved, several thousand system updates per parameter value were simulated before computing the average $\overline{\rho}$. (b) Plots indicating the spatial pattern of different steady states, cloudy (gray) and cloud-free regions (blue), for $p_0 = \{4, 7, 13, 14\}$, hence cloud-free (top left), aggregated with considerable cloud-free areas (top right), aggregated but mostly cloudy (bottom left), and fully cloudy (bottom right).

2.2.3. Case With Spontaneous Generation

We now allow spontaneous generation ($f_{sg} > 0$) and work with the full equation (5), namely,

$$\dot{\rho} = F_{q,p_0,f_{sg}}(\rho)\ , \tag{18}$$

$$F_{q,p_0,f_{sg}}(\rho) \equiv -qp_0\rho^3 + qp_0\rho^2 - \rho(1 + qf_{sg}) + q\ f_{sg}\ . \tag{19}$$

One obvious effect of $f_{sg} > 0$ is to increase the value of the lower stable fixed point, that is, $\rho_1 \approx qf_{sg}$ to linear order, making ρ_1 positive. As a third order polynomial, the zeros of equation (19) are more complicated algebraic expressions (*Details:* Supplement). However, to test for stability of the aggregated state we are again mainly interested in fixed points, where

$$\rho_2 = (\rho_1 + \rho_3)/2 \tag{20}$$

is fulfilled by appropriate adjustment of q. Luckily, the condition on q becomes very simple, namely,

$$q = \frac{9}{2(9f_{sg} + p_0)}\ , \tag{21}$$

which yields equation (12) for $f_{sg} = 0$, as it should. The resulting zeros are also simple, namely,

$$\begin{aligned} \rho_{1/3} &= \frac{1}{3}\left(1 \mp \left(1 - \frac{27f_{sg}}{p_0}\right)^{1/2}\right)\ , \\ \rho_2 &= 1/3\ . \end{aligned} \tag{22}$$

We can quantify the *contrast* $\Delta\rho(p_0, f_{sg})$ between the densities in the aggregated and cloud-sparse regime, as

$$\Delta\rho(p_0, f_{sg}) \equiv \rho_3 - \rho_1 = \frac{2}{3}\left(1 - \frac{27f_{sg}}{p_0}\right)^{1/2}\ , \tag{23}$$

which is sharp for large interaction strength p_0 and small f_{sg}.

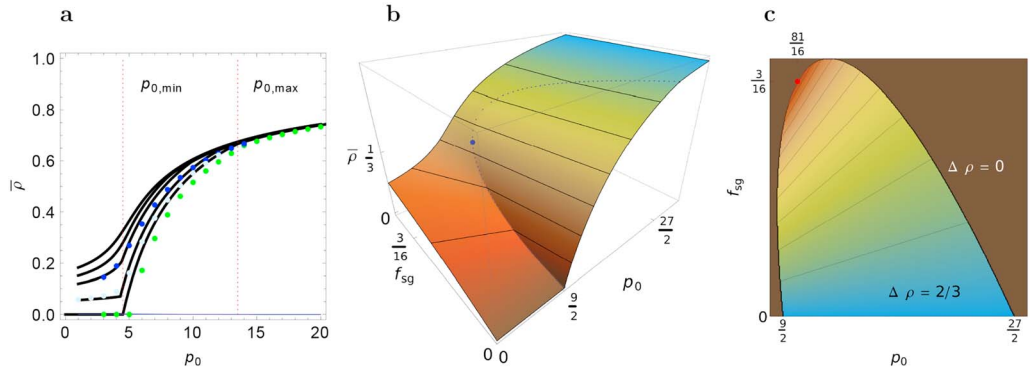

Figure 4. Phase diagram for a system with spontaneous generation. (a) Cloud cover versus interaction strength p_0. Similar to Figure 3a but now allowing for finite spontaneous generation $f_{sg} \geq 0$. Black lines show theoretical results, points of varying colors indicate simulation results on a domain of linear dimension $L = 200$, with simulations carried out as in Figure 3. Curves from bottom to top correspond to $f_{sg} = \{0, .06, .14, 3/16, .24\}$, that is, for the first three we expect a change of slope as function of p_0, for the remaining two we expect smooth behavior. For orientation, the dotted lines indicate the values $p_{0,min}$ and $p_{0,max}$ for the case of $f_{sg} = 0$. (b) Surface plot showing domain average cloud fraction $\overline{\rho}$ versus interaction strength p_0 and spontaneous generation rate f_{sg}. Color shading from orange to blue indicates increasing values of $\overline{\rho}$. Thin black lines are contour lines for several values of $\overline{\rho}$. Dotted line indicates the boundary between nonaggregated (continuum phase) and aggregated convection (clustered phase). Note the abrupt change of slope at the dotted line (most easily visible for $p_0 \approx 9/2$). Note also the "triple point" at $(81/16, 3/16, 1/3)$, marked as a larger blue point, which is characteristic, as it is located at a smooth transition between the continuum and clustered phases. (c) Heatmap of the contrast $\Delta\rho \equiv \rho_3 - \rho_1$, between the densities within and outside the aggregated subdomain. Color shading from orange to blue indicates increasing values of $\Delta\ \rho$. At the "triple point", marked as a red solid circle, $\Delta\ \rho$ vanishes. Figure S1 shows examples of spatial patterns.

However, we have not yet established where this contrast is applicable, as we need the boundaries of the aggregated regime. To obtain this boundary, we again use the condition on q (equation 13), which together with equations (21) and (22) yields the upper and lower lines of transitions $p_0(f_{sg})$ (equations S4 and S5). While these are more elaborate algebraic expressions, they are nonetheless closed and allow us to study the type of transition occurring at the boundaries of the aggregated regime.

Evaluating the expressions for the boundary (equations S4 and S5) together with equation (21), we first compare the previous results for $f_{sg} = 0$ (Figure 3) with those of positive f_{sg} (Figure 4a). The primary effect of increased f_{sg} is to increase total density $\overline{\rho}$. However, for small values of f_{sg}, the slope still changes abruptly when increasing p_0 beyond a threshold. This continuous phase transition signals the entry to the aggregated state (equations S4 and S5). For sufficiently large f_{sg} a change of slope as function of p_0 is no longer observed.

Why does a change of slope occur? Within the aggregated phase, an additional degree of freedom is activated, namely, one where cells lump together to "aid" one another, thus leading to more favorable conditions for replication. At larger values of f_{sg} the discontinuity vanishes—abrupt variations in state are no longer possible. This is explained by f_{sg} diluting free space so strongly that new aggregates will incessantly form all over the domain (compare: Figure 2b).

The figure also shows simulation results for the different parameter combinations. The contrast between theory and simulation is strongest for $f_{sg} = 0$, but also the cases with spontaneous generation display systematic discrepancies. These are partially due to finite system-size effects, whereby at the transition to the aggregated state very small clusters will initially form. These clusters suffer most from the curvature effect (Figure 2a), hence, small clusters will enter a positive feedback loop of decay, where they become smaller and increase the detrimental curvature effect.

Also for larger p_0, at the other end of the aggregated regime, a discontinuity occurs, which is however less noticeable. At this stage, the domain is so densely filled that interaction takes place all over, and clustering is no longer possible. The slope in fact decreases when crossing the threshold (equation S5), a bunched-up state could maintain higher activity, but it becomes statistically impossible to maintain such a segregated state. We summarize the findings for $\overline{\rho}(p_0, f_{sg})$ (Figure 4b) and $c(p_0, f_{sg})$ (equation (23) and Figure 4c).

In summary, edges of the segregated phase within the two-dimensional phase diagram are generally characterized by continuous transitions in $\overline{\rho}$. However, for a single combination of p_0 and f_{sg} this change of slope

should disappear, namely, when $\rho_1 = \rho_2 = \rho_3 = \overline{\rho}$ (*compare*: Figure 2). This point is easy to obtain when using equation (21) and exploiting the equality of densities in equation (22). We thus obtain the "triple point" as

$$f_{sg}^* = \frac{3}{16}\,, \tag{24}$$

$$p_0^* = \frac{81}{16}\,, \tag{25}$$

$$q^* = 2/3 = 1 - \overline{\rho}\,, \tag{26}$$

that is, a point that is characterized by a smooth transition between the continuum and the segregated phases (marked in Figures 4b and 4c). At this point, the contrast (equation (23) and Figure 4c) vanishes.

2.2.4. Including Explicit Spatial Interaction.

As mentioned, our model has assumed some spatial displacement upon collision of cold pools, leading to a formulation where only the number density, not the explicit position of cells in the surroundings of $\mathbf{r}$, was relevant in determining interaction effects between cold pools (Figure 1c). The details of how often and at which precise location cold pools trigger new convective cells is still an open research question. Literature, however, states that cold pools reach typical maximal radii (Black, 1978; Feng et al., 2015; Romps & Jeevanjee, 2016; Zuidema & Li, 2012) and that cold pool interactions often leave behind a new cell near the location of collision (Droegemeier & Wilhelmson, 1985; Feng et al., 2015; Haerter et al., 2018; Holle & Maier, 1980; Tompkins, 2001a; Torri & Kuang, 2018, 2019)—hence, requiring the new cell to lie somewhat in between the centers of the cold pools causing it.

To qualitatively capture such geometric spatial effects, we now consider a refined process on a lattice, where each lattice site represents the area a^*, required by a precipitation cell and its cold pool. In practice, the value of a^* will be a result of a self-organization process, which can be understood as follows: neighboring precipitation cells can instigate new cells, when their respective cold pools have each traveled more than a minimal distance, defined by the radius of the effective precipitation cell area a, but less than the maximal distance r_{max} a cold pool can travel. Typical distances, which define a^*, will lie at intermediate values, and their calculation is a nontrivial statistical mechanics problem, left to a future study. In the current qualitative discussion we take a^* to be a given system parameter.

Given that the site at $\mathbf{r}$ is not occupied, and two neighboring, and spatially opposite sites are occupied by existing cells, for example, cells at $\mathbf{r} - \mathbf{e}_x$ and $\mathbf{r} + \mathbf{e}_x$ (Figure 1d), a new cell can be produced at $\mathbf{r}$ by collision of the cells. Since we only consider neighboring sites for the interaction, we are implicitly assuming that r_{max} is on the order of a lattice site. Note that this type of interaction, where the resulting cell is always produced *between* existing cells, will, for geometrical reasons, be unable to allow boundaries between cloudy and cloud-free areas to grow in favor of the cloudy areas (compare: Figure 2a). In fact, the boundary will gradually retreat and cloud-free "cavities" will tend to increase in size. A single cavity would then grow larger until it takes up the entire domain—no sustainable aggregation could take place. Such a run-away effect will not be physically plausible, since the convective instability would inevitably increase by surface heating and cloud-level radiative cooling. Eventually, other processes, for example, the spontaneous ones discussed throughout the text, or single cold pool processes (Figure 1e) would become active.

We therefore now consider an alternate model, where, in addition to the two cold pool process described, also single cold pool processes are incorporated (Figures 1d and 1e), and the probability for a given vacant site to be "infected" by any occupied neighbor is p_s. We remind the reader that single cold pool processes alone were ruled out on theoretical grounds to give aggregation (discussion following equation (6)). We here test this conclusion numerically (Figure S2a, gray curve). We again initialize our domain with a random seeding of cells and allow the dynamics to evolve. Indeed, for $p_s \gtrsim .1$, $p_0 = 0$, the spreading from any occupied site to its eight nearest neighbors starts to outweigh decay, however, the spatial dynamics yields a random pattern without aggregated clustering (not shown).

We now set $p_0 = 10$, allowing for two-cold pool interaction. Similar to simulations of convective self-aggregation (Wing et al., 2017), the initial effect is that small subregions become cleared from precipitation cells. Some of these cleared regions eventually expand and merge with other cleared region. Finally, only a single cloudy patch remains, which maintains its area indefinitely.

Exploring the parameter p_s systematically, we find that the domain is entirely cloud-free for small values, and a continuous transition to an aggregated regime again exists, similar to the case of $f_{sg} = 0$ for the previous model (Figure 3). With a further increase in p_s, the area of the aggregated subregion further increases. Finally, for very large p_s, aggregation is no longer possible and a featureless cloudy regime is found. For this high-density limit, we could however not detect any phase transition for the order parameter $\overline{\rho}$. Rather, at large values of p_s increasingly diffusive dynamics is found which smoothly leads to a random pattern in space. In summary, also with a stricter condition on the location of cells resulting from the collisions, a phase transition to an aggregated regime is found, when two-cold pool interactions play a sufficient role in generating the new cells.

3. Discussion and Conclusion

Self-aggregation in convection has drawn substantial interest due to its potential applicability to large-scale structures in tropical and subtropical cloud organization, most notably the Madden-Julian Oscillation (Zhang, 2005) in the Indian and Pacific Ocean, as well as the buildup of hurricanes. Cold pool processes are now considered a crucial component in the interaction between convective clouds. However, their exact relation to self-aggregation has been unclear. This may, in part, be due to the large mix of effects, all of which can contribute to the self-organization of the convective cloud field—most prominently the effect of stronger radiative cooling of cloud-free air masses, which has been implicated in the stabilization of a larger-scale circulation pattern to reinforce aggregation (Wing et al., 2017).

With so many effects contributing, the computational demand to map out the entire phase diagram of actual aggregation in fluid-dynamics models is currently prohibitively large. Likely contributors, which would need to be explored, are the value of the sea surface temperature, the ventilation coefficient which describes rain evaporation leading to cold pool formation, model grid resolution, which influences cold pool spreading and the sharpness of gust front boundaries, the radiation and cloud microphysics schemes, as well as domain size and geometry.

This study explored the possible implications of small-scale interactions between clouds. These interactions are active at the spatial scale of cold pool radii, which are typically on the order of tens of kilometers. The model imposed a large-scale energy constraint, by which the propensity of forming new precipitation events is weakened when the large-scale energy budget is used up. Our finding is that when perturbations are weak, in other words, when the main cause of new convective events is the interaction between previous events, mediated through their cold pools, aggregation is likely to occur. For larger perturbations a continuum state would be reached, where the domain shows a rather featureless mix of more cloudy and less cloudy "patchiness."

Notably, our cold pools have been constrained by a maximal radius r_{max}, which sets a scale for cold pool interaction. Increasing r_{max} would correspond to cold pools that can travel larger distances, before their momentum decays. In that case, interactions would become very strong due to the larger value of $\rho(\mathbf{r})$ (equation (3)), and a segregation into an aggregated and a cloud-free phase would no longer occur. In our model (equation (5)), the effect of r_{max} is captured in the parameter p_0, and increases in r_{max} would translate to larger p_0. Hence, for sufficiently large r_{max}, $p_0 > p_{0,max}$, and the aggregation regime in Figure 4 would be left. These considerations are in line with previous findings from simulations (Jeevanjee & Romps, 2013), where self-aggregation was found to be hampered by increased cold pool strength.

In conclusion, we have here introduced a continuum model for convective cell spatial number density as well as a discrete model with explicit spatial interaction, to qualitatively mimic the effect of cold pool interaction within an energy flux constrained framework. When only single cold pools are allowed to set off new convective updrafts, self-aggregation did not occur. Single cold pool processes display a diffusion-like dynamics, which does not constitute a basis for bistability. Conversely, independent of the model, the

interaction between multiple cold pools can indeed give rise to sustained aggregation effects, which self-organize from an initially random cloud distribution.

Acknowledgments
J. O. H. thanks S. J. Boeing, S. B. Nissen, and K. Sneppen as well as the two anonymous reviewers for useful comments. J. O. H. gratefully acknowledge funding by a grant (13168) from the VILLUM Foundation. This project has received funding from the European Research Council (ERC) under the European Union's Horizon 2020 research and innovation program (grant agreement 771859). No new data were used in producing this manuscript.

References

Bak, P., Tang, C., & Wiesenfeld, K. (1987). Self-organized criticality: An explanation of the 1/f noise. *Physical review letters*, *59*(4), 381.
Black, P. G. (1978). Mesoscale cloud patterns revealed by apollo-soyuz photographs. *Bulletin of the American Meteorological Society*, *59*(11), 1409–1419.
Böing, S. J. (2016). An object-based model for convective cold pool dynamics. *Mathematics of Climate and Weather Forecasting*, *2*(1), 43–60.
Bretherton, C. S., Blossey, P. N., & Khairoutdinov, M. (2005). An energy-balance analysis of deep convective self-aggregation above uniform SST. *Journal of the atmospheric sciences*, *62*(12), 4273–4292.
Bretherton, C. S., & Khairoutdinov, M. F. (2015). Convective self-aggregation feedbacks in near-global cloud-resolving simulations of an aquaplanet. *Journal of Advances in Modeling Earth Systems*, *7*, 1765–1787. https://doi.org/10.1002/2015MS000499
Bretherton, C. S., & Smolarkiewicz, P. K. (1989). Gravity waves, compensating subsidence and detrainment around cumulus clouds. *Journal of the atmospheric sciences*, *46*(6), 740–759.
Cahalan, R. F., & Joseph, J. (1989). Fractal statistics of cloud fields. *Monthly Weather Review*, *117*, 261.
Coppin, D., & Bony, S. (2015). Physical mechanisms controlling the initiation of convective self-aggregation in a general circulation model. *Journal of Advances in Modeling Earth Systems*, *7*, 2060–2078. https://doi.org/10.1002/2015MS000571
de Szoeke, S. P., Skyllingstad, E. D., Zuidema, P., & Chandra, A. S. (2017). Cold pools and their influence on the tropical marine boundary layer. *Journal of the Atmospheric Sciences*, *74*(4), 1149–1168.
Droegemeier, K. K., & Wilhelmson, R. B. (1985). Three-dimensional numerical modeling of convection produced by interacting thunderstorm outflows. Part I: Control simulation and low-level moisture variations. *Journal of the atmospheric sciences*, *42*(22), 2381–2403.
Feng, Z., Hagos, S., Rowe, A. K., Burleyson, C. D., Martini, M. N., & de Szoeke, S. P. (2015). Mechanisms of convective cloud organization by cold pools over tropical warm ocean during the AMIE/DYNAMO field campaign. *Journal of Advances in Modeling Earth Systems*, *7*, 357–381. https://doi.org/10.1002/2014MS000384
Goldenfeld, N. (2018). *Lectures on phase transitions and the renormalization group*. Boca Raton, London, New York: CRC Press.
Grabowski, W. W. (2001). Coupling cloud processes with the large-scale dynamics using the cloud-resolving convection parameterization (CRCP). *Journal of the Atmospheric Sciences*, *58*(9), 978–997.
Grant, L. D., & van den Heever, S. C. (2016). Cold pool dissipation. *Journal of Geophysical Research: Atmospheres*, *121*, 1138–1155. https://doi.org/Coldpooldissipation
Haerter, J. O., Böing, S. J., Henneberg, O., & Nissen, S. B. (2018). Reconciling cold pool dynamics with convective self-organization. arXiv:1810.05518v1.
Haerter, J. O., & Schlemmer, L. (2018). Intensified cold pool dynamics under stronger surface heating. *Geophysical Research Letters*, *45*, 6299–6310. https://doi.org/10.1029/2017GL076874
Held, I. M., Hemler, R. S., & Ramaswamy, V. (1993). Radiative-convective equilibrium with explicit two-dimensional moist convection. *Journal of the Atmospheric Sciences*, *50*(23), 3909–3927.
Holle, R. L., & Maier, M. W. (1980). Tornado formation from downdraft interaction in the face mesonetwork. *Monthly Weather Review*, *108*(7), 1010–1028.
Holloway, C. E., Wing, A. A., Bony, S., Muller, C., Masunaga, H., L'Ecuyer, T. S., et al. (2017). Observing convective aggregation. *Surveys in Geophysics*, *38*(6), 1199–1236.
Jeevanjee, N., & Romps, D. M. (2013). Convective self-aggregation, cold pools, and domain size. *Geophysical Research Letters*, *40*, 994–998. https://doi.org/10.1002/grl.50204
Langhans, W., & Romps, D. M. (2015). The origin of water vapor rings in tropical oceanic cold pools. *Geophysical Research Letters*, *42*, 7825–7834. https://doi.org/10.1002/2015GL065623
Lovejoy, S., & Schertzer, D. (2006). Multifractals, cloud radiances and rain. *Journal of Hydrology*, *322*, 59–88.
Moseley, C., Henneberg, O., & Haerter, J. O. (2018). A statistical model for isolated convective precipitation events. *Journal of Advances in Modeling Earth Systems*, *11*, 360–375. https://doi.org/10.1029/2018MS001383
Muller, C., & Bony, S. (2015). What favors convective aggregation and why? *Geophysical Research Letters*, *42*, 5626–5634. https://doi.org/10.1002/2015GL064260
Muller, C. J., & Held, I. M. (2012). Detailed investigation of the self-aggregation of convection in cloud-resolving simulations. *Journal of the Atmospheric Sciences*, *69*(8), 2551–2565.
Peters, O., & Christensen, K. (2002). Rain: Relaxations in the sky. *Physical Review E*, *66*, 036–120.
Peters, O., & Neelin, J. D. (2006). Critical phenomena in atmospheric precipitation. *Nature Physics*, *2*, 293–296.
Romps, D. M., & Jeevanjee, N. (2016). On the sizes and lifetimes of cold pools. *Quarterly Journal of the Royal Meteorological Society*, *142*(696), 1517–1527.
Terai, C., & Wood, R. (2013). Aircraft observations of cold pools under marine stratocumulus. *Atmospheric Chemistry and Physics*, *13*(19), 9899–9914.
Tobin, I., Bony, S., & Roca, R. (2012). Observational evidence for relationships between the degree of aggregation of deep convection, water vapor, surface fluxes, and radiation. *Journal of Climate*, *25*(20), 6885–6904.
Tompkins, A. M. (2001a). Organization of tropical convection in low vertical wind shears: The role of cold pools. *Journal of the Atmospheric Sciences*, *58*(13), 1650–1672.
Tompkins, A. M. (2001b). Organization of tropical convection in low vertical wind shears: The role of water vapor. *Journal of the Atmospheric Sciences*, *58*(6), 529–545.
Torri, G., & Kuang, Z. (2018). On cold pool collisions in tropical boundary layers. *Geophysical Research Letters*, *46*, 399–407. https://doi.org/10.1029/2018GL080501
Torri, G., & Kuang, Z. (2019). On cold pool collisions in tropical boundary layers. *Geophysical Research Letters*, *46*, 399–407. https://doi.org/10.1029/2018GL080501
Windmiller, J. M. (2017). (PhD. thesis), (Ludwig-Maximilian University, Munich Germany).
Wing, A. A., Emanuel, K., Holloway, C. E., & Muller, C. (2017). Convective self-aggregation in numerical simulations: A review. *Surveys in Geophysics*, *38*(6), 1173–1197.
Yeomans, J. M. (1992). *Statistical mechanics of phase transitions*. Oxford: Clarendon Press.
Zhang, C. (2005). Madden-Julian oscillation. *Reviews of Geophysics*, *43*, RG2003. https://doi.org/10.1029/2004RG000158

Zuidema, P., & Li, Z. (2012). On trade wind cumulus cold pools. *Journal of the Atmospheric Sciences*, *69*(1), 258–280.
Zuidema, P., Torri, G., Muller, C., & Chandra, A. (2017). A survey of precipitation-induced atmospheric cold pools over oceans and their interactions with the larger-scale environment. *Surveys in Geophysics*, *38*, 1283–1305.